Progress In Electromagnetics Research C, Vol. 90, 139–154, 2019

Evaluation and Minimization of Cramer-Rao Bound for Conformal Antenna Arrays with Directional Emitters for DOA-Estimation

Yuri Nechaev[1], Ilia Peshkov[2, *], and Natalia Fortunova[2]

Abstract—The Cramer-Rao lower bound (CRLB) for calculating errors and accuracy of direction-of-arrival (DOA) estimation is discussed for a number of planar waves arriving on an antenna array. It is well known that the geometry of antenna arrays imposes restrictions on the performances of the direction-of-arrival estimation. In particular, the influence of the directivity factor of the individual antenna elements on the accuracy of the DOA estimation of the radio emission sources for circular (cylindrical), cubic and spherical antenna arrays consisting of the directional antenna elements is investigated. The directivity factor of antenna elements is changed within wide limits in order to determine the values at which the high accuracy of the direction-finding can be achieved. It is shown that further increasing the directivity factor of each antenna element makes the mean square error in the determination of the coordinates of the signals increase as well. The exact expression for the Cramer-Rao lower bound for the DOA-estimation variance calculation depending on the antenna directivity and the geometry is presented. The obtained exact equation shows the most important factors that the direction-of-arrival estimation accuracy is dependent on. A technique of obtaining antenna arrays with optimal directional elements locations is proposed. Those arrays allow increasing DOA estimation accuracy by several times.

1. INTRODUCTION

Direction-of-arrival estimation of signal sources takes a great interest in such tasks as radars, sonars, and wireless communications [1–6] by using linear antenna arrays. The arrays are simple to implement and understand, but they are not able to execute simultaneous direction-of-arrival estimation in three-dimensional space, i.e., azimuth and elevation [7]. Planar and conformal antenna arrays are capable of overcoming this problem [8–10]. Additionally, many papers assume that the antennas are isotropic [1–10]. Many conformal volume antenna arrays consist of rectangular patch-antenna elements as a rule, which have directivity factor greater than 1. So considering the influence of the directivity factor of a particular antenna element on performances of DOA-estimation is of serious interest. Therefore, the paper focuses on researching three-dimensional conformal antenna arrays such as cylindrical, cubic, sphere, and cone configurations using the MUSIC method. However, the results of comparative computer simulation can be interpreted as a special case; therefore, an instrument is highly needed such as the Cramer-Rao lower bound which is independent of implementation features.

In papers [11, 12], the problem of obtaining the Cramer-Rao lower bound for the azimuth and elevation DOA-estimation using antenna arrays with directional elements is considered. However, these works do not give an exact expression taking into account the position of the source together with the directivity factor of each antenna element. The following is an improved and expanded matrix-vector expression of the Cramer-Rao lower bound taking into account the aforementioned shortcomings.

Received 18 November 2018, Accepted 13 January 2019, Scheduled 28 February 2019

* Corresponding author: Ilia Peshkov (ilvpeshkov@gmail.com).

[1] Department of Information Systems, Voronezh State University, Voronezh 394000, Russia. [2] Department of Physics, Radio Engineering and Electronics, Bunin Yelets State University, Yelets 399770, Russia.

Additionally, the obtained equation will be very helpful for analyzing the important factors which determine the DOA-estimation accuracy by using antenna arrays of these kinds. Impact on these factors will help us to generate such configuration that will have better characteristics for accuracy and resolution of DOA methods such as MUSIC. Although the idea of optimum antenna elements placements is not new [13, 14], the presented paper allows estimating and analyzing any antenna array composed of directional sensors manually. Additionally, it takes into account the influence of the directivity factor on DOA estimation, and the further obtained equations are simple to realize and use.

2. BUILDING AN ANTENNA ARRAY

2.1. Cubic Antenna Array

Figure 1 shows an array of N rectangular directional elements distributed in space, forming a cubic antenna array. Let us consider the narrow-band signal $s(t)$ on the carrier frequency of ω_0 with the angular coordinates θ and φ with respect to the x-, y- and z-axes, respectively, i.e., θ is related to the azimuth and φ related to the vertical planes. Thus, the task of radio direction-finding is to estimate θ and φ coordinates. It requires the model of the antenna array.

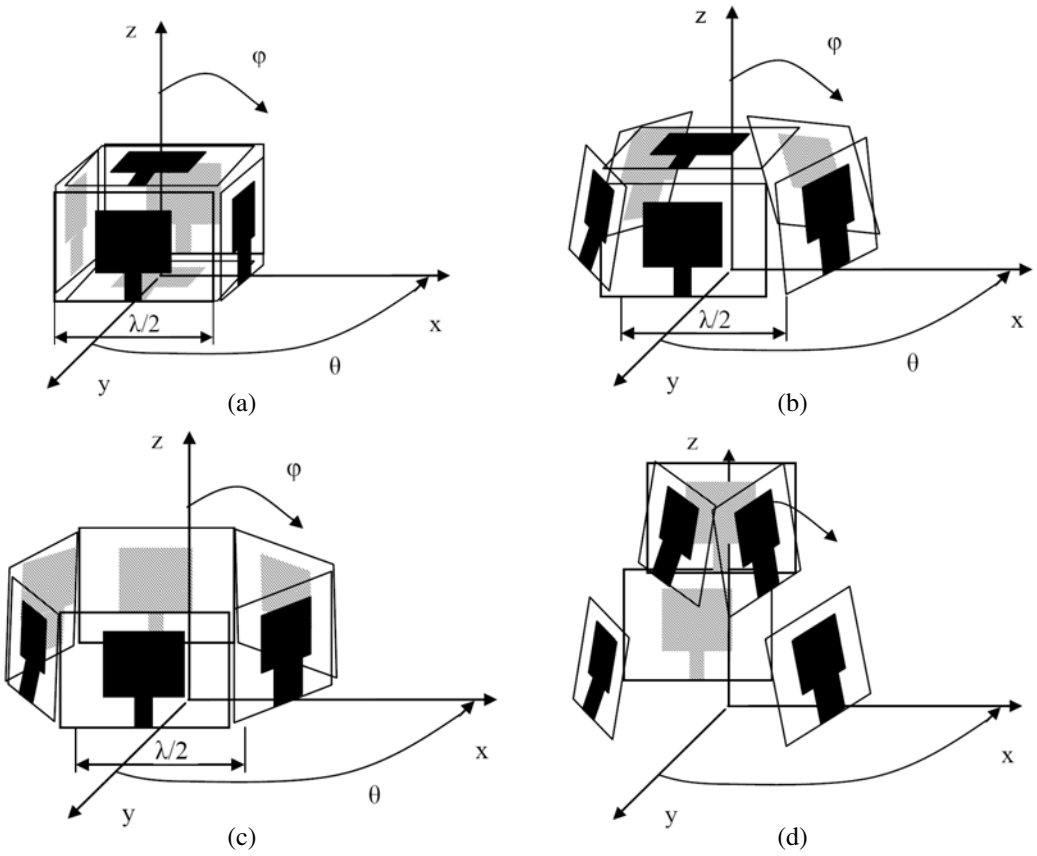

Figure 1. The antenna arrays schemes.

Let us denote $g_i(\omega, \theta, \varphi)$ gain depending on the frequency and direction. Then the analytical signal at the array output is [10]:

$$\mathbf{a}(\omega,\theta,\lambda) = \left[\begin{array}{cccc} g_1(\omega,\theta,\lambda)e^{j\mathbf{kr}_1^T} & g_2(\omega,\theta,\lambda)e^{j\mathbf{kr}_2^T} & \ldots & g_N(\omega,\theta,\lambda)e^{j\mathbf{kr}_N^T} \end{array} \right] \quad (1)$$

where $\mathbf{k} = \frac{2\pi}{\lambda}(k_x, k_y, k_z) = (\sin\varphi\cos\theta, \sin\varphi\sin\theta, \cos\varphi)$ is the wave number, describing the rate of change of the phase of the propagating wave in directions x, y, z. $\mathbf{r}_n^T = (x_n, y_n, z_n)^T$ is the radius-vector

to the n-th antenna and $g_n(\theta,$ and $\varphi)$ is the gain coefficient of the n-th element. Therefore, the steering vector of the antenna array can be expressed as follows:

$$\mathbf{a}(\theta,\varphi)=\begin{bmatrix} g_1(\theta,\varphi+\varphi_1)e^{j\mathbf{k}\mathbf{r}_1^T} \\ g_2(\theta,\varphi)e^{j\mathbf{k}\mathbf{r}_2^T} \\ g_3(\theta+\theta_3,\varphi)e^{j\mathbf{k}\mathbf{r}_3^T} \\ g_4(\theta+\theta_4,\varphi)e^{j\mathbf{k}\mathbf{r}_4^T} \\ g_5(\theta+\theta_5,\varphi)e^{j\mathbf{k}\mathbf{r}_5^T} \\ g_6(\theta,\varphi-\varphi_6)e^{j\mathbf{k}\mathbf{r}_6^T} \end{bmatrix}=\begin{bmatrix} g_1\left(\theta,\varphi+\dfrac{\pi}{2}\right)e^{j\mathbf{k}[0,0,0]^T} \\ g_2(\theta,\varphi)e^{j\mathbf{k}[\frac{\lambda}{4},0,\frac{\lambda}{4}]^T} \\ g_3\left(\theta+\dfrac{\pi}{2},\varphi\right)e^{j\mathbf{k}[0,-\frac{\lambda}{4},\frac{\lambda}{4}]^T} \\ g_4(\theta+\pi,\varphi)e^{j\mathbf{k}[-\frac{\lambda}{4},0,\frac{\lambda}{4}]^T} \\ g_5\left(\theta+\dfrac{3\pi}{2},\varphi\right)e^{j\mathbf{k}[0,\frac{\lambda}{4},\frac{\lambda}{4}]^T} \\ g_6\left(\theta,\varphi-\dfrac{\pi}{2}\right)e^{j\mathbf{k}[0,0,\frac{\lambda}{2}]^T} \end{bmatrix} \tag{2}$$

The construction of the steering vector of the cubic antenna array has been carried out in such a way that the first element is located at the origin of coordinates, i.e., $\mathbf{r}_1^T=[0,0,0]^T$, and is directed by the radiating element along the z-axis, so it has the radiation maximum in the angle of elevation shifted by $+\pi/2$. In the above-mentioned model, the gain coefficient $g_n(\theta,\varphi)$ depends on the azimuth φ coordinate and the angle of elevation θ of the observer. In addition, it is assumed that the radiation maximum is reached at $\theta=0^\circ$ and $\varphi=0^\circ$, and the minimum at $\varphi=90^\circ$, $\theta=0^\circ$, or $\varphi=90^\circ$, $\theta=90^\circ$, as shown in the following math model of power directivity pattern in the far-field assuming that the antennas are perfectly matched and lossless [11]:

$$G(\theta,\varphi)=\frac{D}{2^{2m}}\left(1+\sin\left(\varphi-\gamma_n^{\varphi}\right)\right)^m\left(1+\cos\left(\theta-\gamma_n^{\theta}\right)\right)^m,\quad n=0,1,\ldots,N-1 \tag{3}$$

where γ_n^{φ} and γ_n^{θ} are shifts in the elevation and azimuth planes of n-th antenna, respectively, then $g=\sqrt{G(\theta,\varphi)}$.

The second element has the radius-vector $\mathbf{r}_2^T=\left[\frac{\lambda}{4},0,\frac{\lambda}{4}\right]^T$, because the width of each radiator is half-wavelength. The locations of other radiators are calculated in a similar way.

2.2. Half-Dodecahedron Antenna Array

Figure 1(b) shows the antenna array in the form of a half-dodecahedron, and the length of the side is equal to $\lambda/2$. The half-dodecahedron has two parameters: the radii of the incircle and circumcircle, which are respectively equal to $r_{in}=1,\ 1\lambda/2$ and $r_{out}=1,\ 4\lambda/2$. In total, there are six elements, with five around the circumference. The angle between them is 72°. The angle between the upper face and any lateral one (antenna elements) is 116°.

Then, the steering vector of the antenna array can be expressed as:

$$\mathbf{a}(\theta,\varphi)=\begin{bmatrix} g_1(\theta,\varphi+\varphi_1)e^{j\mathbf{k}\mathbf{r}_1^T} \\ g_2(\theta+\theta_2,\varphi+\varphi_2)e^{j\mathbf{k}\mathbf{r}_2^T} \\ g_3(\theta+\theta_3,\varphi+\varphi_3)e^{j\mathbf{k}\mathbf{r}_3^T} \\ g_4(\theta+\theta_4,\varphi+\varphi_4)e^{j\mathbf{k}\mathbf{r}_4^T} \\ g_5(\theta+\theta_5,\varphi+\varphi_5)e^{j\mathbf{k}\mathbf{r}_5^T} \\ g_6(\theta+\theta_6,\varphi+\varphi_6)e^{j\mathbf{k}\mathbf{r}_6^T} \end{bmatrix}=\begin{bmatrix} g_1\left(\theta,\varphi+\dfrac{\pi}{2}\right)e^{j\mathbf{k}\mathbf{R}_z(0)[0,0,r_{in}]^T} \\ g_2\left(\theta+\dfrac{\pi}{2.5},\varphi+\dfrac{\pi}{6.8}\right)e^{j\mathbf{k}\mathbf{R}_z\left(\frac{\pi}{2.5}\right)[0,r_{out},\frac{r_{in}}{2}]^T} \\ g_3\left(\theta+2\dfrac{\pi}{2.5},\varphi+\dfrac{\pi}{6.8}\right)e^{j\mathbf{k}\mathbf{R}_z\left(2\frac{\pi}{2.5}\right)[0,r_{out},\frac{r_{in}}{2}]^T} \\ g_4\left(\theta+2\dfrac{\pi}{2.5},\varphi+\dfrac{\pi}{6.8}\right)e^{j\mathbf{k}\mathbf{R}_z\left(3\frac{\pi}{2.5}\right)[0,r_{out},\frac{r_{in}}{2}]^T} \\ g_5\left(\theta+4\dfrac{\pi}{2.5},\varphi+\dfrac{\pi}{6.8}\right)e^{j\mathbf{k}\mathbf{R}_z\left(4\frac{\pi}{2.5}\right)[0,r_{out},\frac{r_{in}}{2}]^T} \\ g_1\left(\theta+5\dfrac{\pi}{2.5},\varphi+\dfrac{\pi}{6.8}\right)e^{j\mathbf{k}\mathbf{R}_z\left(5\frac{\pi}{2.5}\right)[0,r_{out},\frac{r_{in}}{2}]^T} \end{bmatrix} \tag{4}$$

where $\mathbf{R}_z(\theta)=\begin{bmatrix} \cos\theta & -\sin\theta & 0 \\ \sin\theta & \cos\theta & 0 \\ 0 & 0 & 1 \end{bmatrix}$ is the rotation matrix around the z-axis, simplifying the construction.

2.3. Cylindrical Antenna Array

Here, the steering vector of m-th radio emission source on the n-th antenna element (Fig. 1(c)) in terms of the azimuth and elevation angles, as well as the position of the array elements becomes:

$$\mathbf{a}(\theta,\varphi)=\begin{bmatrix} g_1(\theta,\varphi)e^{j\mathbf{k}\mathbf{r}_1^T} \\ g_2(\theta+\theta_2,\varphi)e^{j\mathbf{k}\mathbf{r}_2^T} \\ g_3(\theta+\theta_3,\varphi)e^{j\mathbf{k}\mathbf{r}_3^T} \\ g_4(\theta+\theta_4,\varphi)e^{j\mathbf{k}\mathbf{r}_4^T} \\ g_5(\theta+\theta_5,\varphi)e^{j\mathbf{k}\mathbf{r}_5^T} \\ g_6(\theta+\theta_6,\varphi)e^{j\mathbf{k}\mathbf{r}_6^T} \end{bmatrix}=\begin{bmatrix} g_1(\theta,\varphi)e^{j\mathbf{k}\mathbf{R}_z(0)[0,r_{circ},\frac{\lambda}{4}]^T} \\ g_2\left(\theta+\dfrac{2\pi}{N},\varphi\right)e^{j\mathbf{k}\mathbf{R}_z\left(\frac{2\pi}{N}\right)[0,r_{circ},\frac{\lambda}{4}]^T} \\ g_3\left(\theta+2\dfrac{2\pi}{N},\varphi\right)e^{j\mathbf{k}\mathbf{R}_z\left(2\frac{2\pi}{N}\right)[0,r_{circ},\frac{\lambda}{4}]^T} \\ g_4\left(\theta+3\dfrac{2\pi}{N},\varphi\right)e^{j\mathbf{k}\mathbf{R}_z\left(3\frac{2\pi}{N}\right)[0,r_{circ},\frac{\lambda}{4}]^T} \\ g_5\left(\theta+4\dfrac{2\pi}{N},\varphi\right)e^{j\mathbf{k}\mathbf{R}_z\left(4\frac{2\pi}{N}\right)[0,r_{circ},\frac{\lambda}{4}]^T} \\ g_1\left(\theta+5\dfrac{2\pi}{N},\varphi\right)e^{j\mathbf{k}\mathbf{R}_z\left(5\frac{2\pi}{N}\right)[0,r_{circ},\frac{\lambda}{4}]^T} \end{bmatrix} \tag{5}$$

where $r_{circ}=\frac{\sqrt{3}}{2}\frac{\lambda}{2}$. The conical array can be considered as a special case of the cylindrical antenna array (Fig. 1(d)). In this case, the conical array will consist of two tiers of the cylindrical antenna array, and each of them will contain $N=3$ elements. In this case, the radius of the lower tier is greater than the radius of the upper tier, i.e., $r_{circ1}>r_{circ2}$, and there are patch antennas turn in the φ plane. Thus, the steering vector of the conical array becomes:

$$\mathbf{a}(\theta,\varphi)=\begin{bmatrix} \dfrac{\mathbf{a}_{circ1}(\theta,\varphi)}{\mathbf{a}_{circ2}(\theta,\varphi)} \end{bmatrix}=\begin{bmatrix} g_1\left(\varphi,\theta+\dfrac{\pi}{6.8}\right)e^{j\mathbf{k}\mathbf{R}_z(0)\mathbf{r}_1^T} \\ g_2\left(\varphi+\dfrac{2\pi}{N},\theta+\dfrac{\pi}{6.8}\right)e^{j\mathbf{k}\mathbf{R}_z\left(\frac{2\pi}{N}\right)\mathbf{r}_1^T} \\ g_3\left(\varphi+2\dfrac{2\pi}{N},\theta+\dfrac{\pi}{6.8}\right)e^{j\mathbf{k}\mathbf{R}_z\left(2\frac{2\pi}{N}\right)\mathbf{r}_1^T} \\ g_4\left(\varphi,\theta+\dfrac{\pi}{6.8}\right)e^{j\mathbf{k}\mathbf{R}_z(0)\mathbf{r}_2^T} \\ g_5\left(\varphi+\dfrac{2\pi}{N},\theta+\dfrac{\pi}{6.8}\right)e^{j\mathbf{k}\mathbf{R}_z\left(\frac{2\pi}{N}\right)\mathbf{r}_2^T} \\ g_6\left(\varphi+2\dfrac{2\pi}{N},\theta+\dfrac{\pi}{6.8}\right)e^{j\mathbf{k}\mathbf{R}_z\left(2\frac{2\pi}{N}\right)\mathbf{r}_2^T} \end{bmatrix} \tag{6}$$

where $\mathbf{r}_1=\begin{bmatrix} 0 & r_{circ1} & \frac{\lambda}{4} \end{bmatrix}^T$ and $\mathbf{r}_2=\begin{bmatrix} 0 & r_{circ2} & \frac{3\lambda}{4} \end{bmatrix}^T$.

As we can see, there is no gap between the elements with considered dimensions of the radiators in all configurations of antenna arrays. However, it is possible to achieve such radii to find approximately the same area of antenna elements. In all cases, the number of antenna elements is $N=6$.

3. THE CRAMER-RAO LOWER BOUND FOR ANTENNA ARRAYS WITH DIRECTIONAL ELEMENTS

Suppose that we have a vector $\tilde{\mathbf{x}}(t)$, forming a stationary Gaussian process with zero mean having moments of the this kind:

$$E\left\{\vec{\mathbf{x}}(t)\vec{\mathbf{x}}^H(t)\right\}=\mathbf{R}\delta_{ij}=\left(\mathbf{A}\mathbf{S}\mathbf{A}^H+\sigma^2\mathbf{I}\right)\delta_{ij} \tag{7}$$

where $\mathbf{S}$ is the signal correlation matrix, $\mathbf{A}$ the steering matrix, σ^2 the noise power, and noise is Gaussian as well.

The likelihood function of the i.i.d. samples $\tilde{\mathbf{x}}(t_1),\ldots\tilde{\mathbf{x}}(t_N)$ is expressed as the negative log-likelihood function:

$$l\left(\theta,\mathbf{S},\sigma^2\right)=N\log|\mathbf{R}|+-\sum_{i=1}^{N}\mathbf{x}^H(t_i)\,\mathbf{R}^{-1}\mathbf{x}(t_i)=\log|\mathbf{R}|+Tr\left\{\mathbf{R}^{-1}\hat{\mathbf{R}}\right\} \tag{8}$$

where $|\ldots|$ — the matrix determinant.

The Cramer-Rao lower bound (CRLB) is an important measurement parameter which shows how well a method works. Suppose that $\hat{\boldsymbol{\eta}}$ is unbiased estimation of the parameter vector $\boldsymbol{\eta}_0$, i.e., $E\{\hat{\eta}\} = \boldsymbol{\eta}_0$ based on samples $\mathbf{X}_N$, then the lower bound:

$$E\left\{(\hat{\boldsymbol{\eta}} - \boldsymbol{\eta}_0)(\hat{\boldsymbol{\eta}} - \boldsymbol{\eta}_0)^T\right\} \geq \left[-E\left\{\frac{\partial^2 \log p(\mathbf{X}_N|\boldsymbol{\eta})}{\partial \boldsymbol{\eta} \partial \boldsymbol{\eta}^T}\right\}\right]^{-1} \tag{9}$$

The compact expression for CRLB for P parameters of M signals is easily deduced from Eq. (9). For the case if only one parameter ($p = 1$) is associated with each signal (as an example: azimuth angle), the CRLB can be written [15]:

$$\mathbf{B}_{STO} = \frac{\sigma^2}{2N}\Re\left[Tr\left\{\left(\mathbf{D}^H\mathbf{P}_A^{\perp}\mathbf{D}\right) \circ \left(\mathbf{S}\mathbf{A}^H\mathbf{R}^{-1}\mathbf{A}\mathbf{S}\right)^T\right\}\right]^{-1} \tag{10}$$

where $\circ$ — element-wise multiplication, $\mathbf{D}$ is the matrix of derivatives of the steering vectors in Eqs. (2)–(6), and $\mathbf{P}_{\mathbf{A}}^{\perp}$ is the orthogonal projection onto the null space $\mathbf{A}^H$. An idea in [15] is used to adopt CRLB of Eq. (10) to an arbitrary number of signals and their parameters (first of all, azimuth and elevation DOA). First we need to define $\mathbf{D}_\theta$, $\mathbf{D}_\varphi$ [10]:

$$\mathbf{D}_{\theta,\varphi} = \left[\left.\frac{\partial \mathbf{a}(\theta_1,\varphi_1)}{\partial \eta}\right|_{\eta=\theta_1,\varphi_1}, \ldots, \left.\frac{\partial \mathbf{a}(\theta_d,\varphi_d)}{\partial \eta}\right|_{\eta=\theta_d,\varphi_d}\right] \tag{11}$$

Thus, the covariance matrix of error of 3D DOA estimation:

$$\mathbf{B}_{STO} = \frac{\sigma^2}{2N}\Re\left[Tr\left\{\begin{bmatrix}\Lambda_1 & \Lambda_2\\ \Lambda_3 & \Lambda_4\end{bmatrix} \circ \begin{bmatrix}\Xi & \Xi\\ \Xi & \Xi\end{bmatrix}^T\right\}\right]^{-1} \tag{12}$$

where $\boldsymbol{\Lambda}_1 = \mathbf{D}_\theta^H\mathbf{P}_A^{\perp}\mathbf{D}_\theta$, $\boldsymbol{\Lambda}_2 = \mathbf{D}_\theta^H\mathbf{P}_A^{\perp}\mathbf{D}_\varphi$, $\boldsymbol{\Lambda}_3 = \mathbf{D}_\varphi^H\mathbf{P}_A^{\perp}\mathbf{D}_\theta$, $\boldsymbol{\Lambda}_4 = \mathbf{D}_\varphi^H\mathbf{P}_A^{\perp}\mathbf{D}_\varphi$, $\Xi = \mathbf{S}\mathbf{A}^H\mathbf{R}^{-1}\mathbf{A}\mathbf{S}$.

Using Eq. (1), the partial derivatives of a vector $\mathbf{a}(\theta_m,\varphi_m)$ from θ and φ [16]:

$$\left.\begin{array}{l}\dfrac{\partial \mathbf{a}(\theta_m,\varphi_m)}{\partial \eta} = \dfrac{\partial g(\theta_m,\varphi_m)\, e^{j\mathbf{k}_m\mathbf{R}^T}}{\partial \eta} = \\ \dfrac{\partial g(\theta_m,\varphi_m)}{\partial \eta} e^{j\mathbf{k}_m\mathbf{R}^T} + g(\theta_m,\varphi_m)\dfrac{\partial e^{j\mathbf{k}_m\mathbf{R}^T}}{\partial \eta}\end{array}\right|_{\eta=\theta_m,\varphi_m} \tag{13}$$

Next, it is necessary to determine the expressions for the derivatives for the phase and amplitude components. First, we define the derivative of the exponential part on azimuth for the k-th signal on the n-th antenna element:

$$\begin{array}{l}\dfrac{\partial e^{j\psi}}{\partial \theta_k} = \dfrac{\partial j\psi}{\partial \theta_k} e^{j\psi} = \dfrac{\partial j\dfrac{2\pi}{\lambda}(x_n k_x + y_n k_y + z_n k_z)}{\partial \theta_k} e^{j\left(\frac{2\pi}{\lambda}(x_n k_x + y_n k_y + z_n k_z)\right)} = \\ j\left(\dfrac{2\pi}{\lambda}(-x_n \sin\theta \sin\varphi + y_n \cos\theta \sin\varphi)\right) e^{j\left(\frac{2\pi}{\lambda}(x_n \cos\theta \sin\varphi + y_n \sin\theta \sin\varphi + z_n \cos\varphi)\right)}\end{array} \tag{14}$$

Define the derivative of the exponential part on elevation and azimuth for the k-th signal on the n-th antenna element:

$$\begin{array}{l}\dfrac{\partial e^{j\psi}}{\partial \varphi_k} = \dfrac{\partial j\psi}{\partial \varphi_k} e^{j\psi} = \dfrac{\partial j\dfrac{2\pi}{\lambda}(x_n k_x + y_n k_y + z_n k_z)}{\partial \varphi_k} e^{j\left(\frac{2\pi}{\lambda}(x_n k_x + y_n k_y + z_n k_z)\right)} = \\ j\left(\dfrac{2\pi}{\lambda}(x_n \cos\theta \cos\varphi + y_n \sin\theta \cos\varphi - z_n \sin\theta)\right) e^{j\left(\frac{2\pi}{\lambda}(x_n \cos\theta \sin\varphi + y_n \sin\theta \sin\varphi + z_n \cos\theta)\right)}\end{array} \tag{15}$$

We define the derivative of the amplitude component with respect to the azimuth and elevation angle for the k-th signal on the n-th antenna element respectively:

$$\frac{\partial g_n(\varphi_k,\theta_k)}{\partial\theta_k} = \frac{\partial}{\partial\theta_k}\frac{D}{2^{2m}}(1+\sin(\varphi_k-\varphi_n))^m(1+\cos(\theta_k-\theta_n))^m = \frac{D}{2^{2m}}(1+\sin(\varphi_k-\varphi_n))^m\frac{\partial}{\partial\theta_k}[(1+\cos(\theta_k-\theta_n))^m] = \frac{D}{2^{2m}}(1+\sin(\varphi_k-\varphi_n))^m\left[m(1+\cos(\theta_k-\theta_n))^{m-1}(-\theta_n)(-\sin(\theta_k-\theta_n))\right] \tag{16}$$

and

$$\frac{\partial g_n(\varphi_k,\theta_k)}{\partial\varphi_k} = \frac{\partial}{\partial\varphi_k}\frac{D}{2^{2m}}(1+\sin(\varphi_k-\varphi_n))^m(1+\cos(\theta_k-\theta_n))^m = \frac{D}{2^{2m}}\left[\frac{\partial}{\partial\varphi_k}(1+\sin(\varphi_k-\varphi_n))^m\right](1+\cos(\theta_k-\theta_n))^m = \frac{D}{2^{2m}}\left[m(1+\sin(\varphi_k-\varphi_n))^{m-1}(-\varphi_n)\cos(\varphi-\varphi_k)\right](1+\cos(\theta_k-\theta_n))^m \tag{17}$$

Substituting expressions (14)–(17) in (13), we derive a matrix-vector expression for calculating the Cramer-Rao lower bound for estimating an arbitrary number of sources in the azimuth and elevation planes on an arbitrary antenna array taking into account of the directivity factor.

3.1. Theoretical Researching

Consider now the CRLB, depending on the directivity factor for cylindrical, cubic, conical and sphere-shaped antenna arrays, each of which consists of six elements (Fig. 1). In these cases, the directivity factor changes from two to six to determine the effect of the antenna beam pattern on the accuracy of

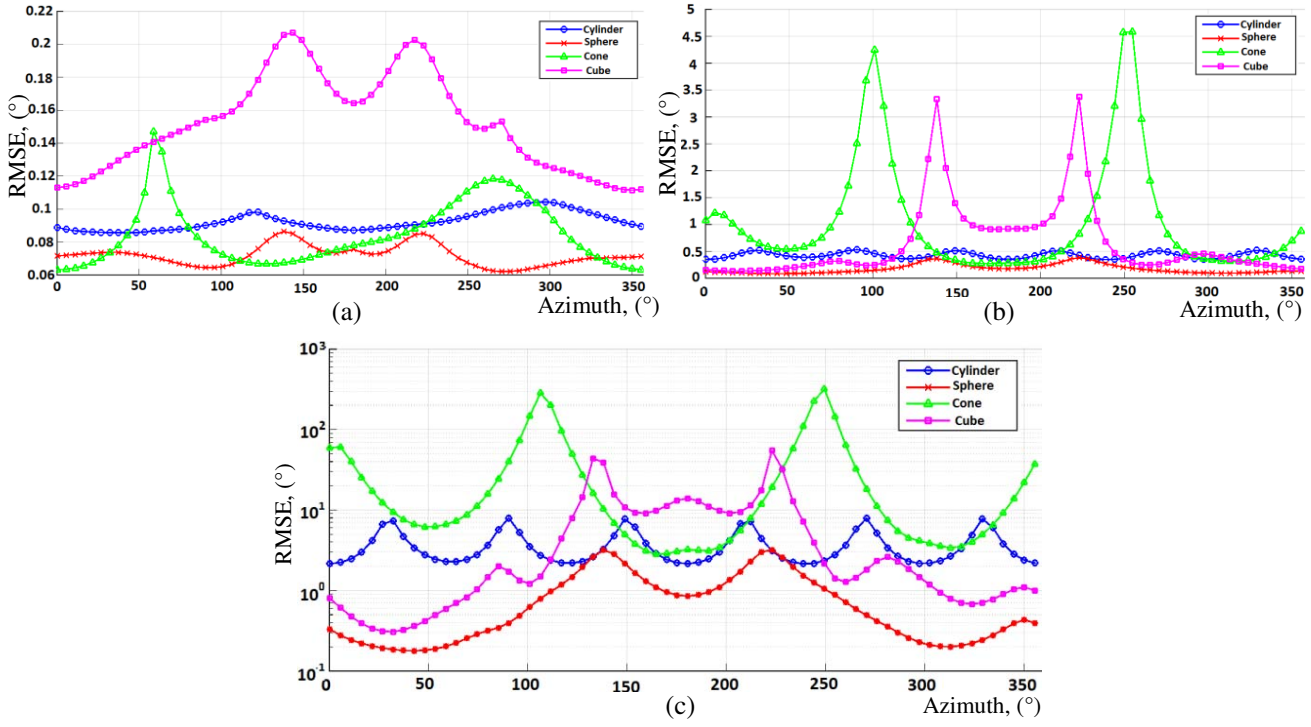

Figure 2. CRLB of the antenna arrays for the directivity factors: (a) $D = 2$, (b) $D = 4$ and (c) $D = 6$.

direction finding, using Eqs. (12)–(13), more clearly. Additionally, the elevation angular coordinate is fixed to 45°, and the azimuth varies from 0° to 360°.

From Fig. 2 we can conclude that firstly, the oscillation amplitude of DOA-estimation errors becomes more obvious and sharp if the directivity factor increases from two to six. This behavior is influenced by falling the signal into the nulls of the radiation patterns, as we will see in detail further. Secondly, the best antenna array geometry with directional patch-antennas for DOA-estimation on azimuth and elevation is sphere (half dodecahedron, Fig. 1(b)). However, the errors distribution is rather flat even if the directivity factor is big (Fig. 2(c)). Thirdly, the cone and cubic antenna arrays produce significant leaps in DOA estimations depending on the signal source location in the azimuth plane.

4. THE EXACT EQUATION OF THE CRAMER-RAO LOWER BOUND FOR ANTENNA ARRAYS WITH DIRECTIONAL ELEMENTS

4.1. One Signal and Two Antennas Case

Consider a case here that a particular antenna array consists of two directional antenna elements and then:

$$\mathbf{a} = \begin{bmatrix} g_1 e^{j\mathbf{k}\mathbf{r}_1^T} & g_2 e^{j\mathbf{k}\mathbf{r}_2^T} \end{bmatrix} \tag{18}$$

Here and further we assume that $a = e^{j\mathbf{k}\mathbf{r}_1^T}$, $a' = \frac{\partial j\mathbf{k}_1\mathbf{R}^T}{\partial\eta}$ and $g' = \frac{\partial g(\theta_m,\varphi_m)}{\partial\eta}$, then

$$\frac{\partial\mathbf{a}\left(\theta_m,\varphi_m\right)}{\partial\eta} = g'a + ga'_a \tag{19}$$

In order to obtain the exact equation of the Cramer-Rao lower bound we need to know the vector of derivatives of the steering vector, i.e.,

$$\mathbf{b} = \frac{\partial\mathbf{a}}{\partial\eta} = \begin{bmatrix} \frac{\partial a_1}{\partial\eta} & \frac{\partial a_2}{\partial\eta} \end{bmatrix}^T = \begin{bmatrix} \frac{\partial g_1 a_1}{\partial\eta} & \frac{\partial g_2 a_2}{\partial\eta} \end{bmatrix}^T = \begin{bmatrix} g'_1 a_1 + g_1 a'_1 a_1 & g'_2 a_2 + g_2 a'_2 a_2 \end{bmatrix}^T \tag{20}$$

$$\mathbf{b}^H = \left(\frac{\partial\mathbf{a}}{\partial\eta}\right)^H = \begin{bmatrix} \left(\frac{\partial a_1}{\partial\eta}\right)^H & \left(\frac{\partial a_2}{\partial\eta}\right)^H \end{bmatrix}^T = \begin{bmatrix} \left(\frac{\partial g_1 a_1}{\partial\eta}\right)^H & \left(\frac{\partial g_2 a_2}{\partial\eta}\right)^H \end{bmatrix} = \begin{bmatrix} \left(g'_1 a_1 + g_1 a'_1 a_1\right)^H & \left(g'_2 a_2 + g_2 a'_2 a_2\right)^H \end{bmatrix}^T = \begin{bmatrix} g'_1 a_1^H + g_1 \left(a'_1 a_1\right)^H & g'_2 a_2^H + g_2 \left(a'_2 a_2\right)^H \end{bmatrix}^T \tag{21}$$

As we can see, Equation (12) is rather complicated, and here we consider only one particular case. Then after simplifying Eq. (12), CRLB for the case of only one signal source can be expressed as follows:

$$\mathrm{var}(\varphi,\theta) = \frac{\sigma^2}{2K}\Re\left[\left(\frac{\partial\mathbf{a}^H}{\partial\eta}\left(\mathbf{I} - \mathbf{a}\left(\mathbf{a}^H\mathbf{a}\right)^{-1}\mathbf{a}^H\right)\frac{\partial\mathbf{a}}{\partial\eta}\right)\circ\Xi\right]^{-1} \tag{22}$$

Equation (22) can be rewritten more compactly as follows [17]:

$$\mathrm{var}(\varphi,\theta) = \frac{\sigma^2}{2KP_s}\frac{1}{AR}\left(\frac{\lambda}{2\pi}\right)^2 \tag{23}$$

Consider the right-hand side of expressions (22)–(23) more deeply. They consist of two factors. As already noted, $\Xi \approx P_S$ for a single source case under the consideration, then we take a closer look at the rest:

$$\begin{aligned} \left[\mathbf{D}_{\theta,\varphi}^H\mathbf{P}_A^{\perp}\mathbf{D}_{\theta,\varphi}\right] &= \left[\frac{\partial\mathbf{a}^H}{\partial\eta}\left(\mathbf{I} - \mathbf{a}\left(\mathbf{a}^H\mathbf{a}\right)^{-1}\mathbf{a}^H\right)\frac{\partial\mathbf{a}}{\partial\eta}\right] \\ &= \begin{bmatrix} \left(g'_1 a_1 + g_1 a'_1 a_1\right)^H & \left(g'_2 a_2 + g_2 a'_2 a_2\right)^H \end{bmatrix}\mathbf{P}_A^{\perp}\begin{bmatrix} g'_1 a_1 + g_1 a'_1 a_1 \\ g'_2 a_2 + g_2 a'_2 a_2 \end{bmatrix} \end{aligned} \tag{24}$$

Consider the exact expression for the component $\mathbf{P}_A^{\perp}$:

$$\begin{aligned}\mathbf{P}_A^{\perp} &= \begin{bmatrix} 1 & 0 \\ 0 & 1 \end{bmatrix} - \begin{bmatrix} a_1 \\ a_2 \end{bmatrix} \left[\begin{bmatrix} a_1^H & a_2^H \end{bmatrix} \begin{bmatrix} a_1 \\ a_2 \end{bmatrix} \right]^{-1} \begin{bmatrix} a_1^H & a_2^H \end{bmatrix} \\ &= \begin{bmatrix} 1 & 0 \\ 0 & 1 \end{bmatrix} - \begin{bmatrix} g_1 a_1 \\ g_2 a_2 \end{bmatrix} \left[\begin{bmatrix} g_1 a_1^H & g_2 a_2^H \end{bmatrix} \begin{bmatrix} g_1 a_1 \\ g_2 a_2 \end{bmatrix} \right]^{-1} \begin{bmatrix} g_1 a_1^H & g_2 a_2^H \end{bmatrix} \\ &= \begin{bmatrix} 1 & 0 \\ 0 & 1 \end{bmatrix} - \frac{1}{g_1^2 + g_2^2} \begin{bmatrix} g_1^2 & g_1 g_2 a_1 a_2^H \\ g_2 g_1 a_2 a_1^H & g_2^2 \end{bmatrix} = \frac{1}{g_1^2 + g_2^2} \begin{bmatrix} g_2^2 & -g_1 g_2 a_1 a_2^H \\ -g_2 g_1 a_2 a_1^H & g_1^2 \end{bmatrix} \end{aligned} \tag{25}$$

Consider the result of multiplying the matrix $\mathbf{P}_A^{\perp}$ on the right-hand side of formula (24):

$$\begin{aligned} &\frac{1}{g_1^2 + g_2^2} \begin{bmatrix} (g'_1 a_1 + g_1 a'_1 a_1)^H & (g'_2 a_2 + g_2 a'_2 a_2)^H \end{bmatrix} \\ &\begin{bmatrix} g_2^2 (g'_1 a_1 + g_1 a'_1 a_1) - g_1 g_2 a_1 a_2^H (g'_2 a_2 + g_2 a'_2 a_2) \\ -g_2 g_1 a_2 a_1^H (g'_1 a_1 + g_1 a'_1 a_1) + g_1^2 (g'_2 a_2 + g_2 a'_2 a_2) \end{bmatrix} = \\ &\frac{1}{g_1^2 + g_2^2} \begin{bmatrix} \left(g_2^2 (g'_1 a_1 + g_1 a'_1 a_1) - g_1 g_2 a_1 a_2^H (g'_2 a_2 + g_2 a'_2 a_2)\right) (g'_1 a_1 + g_1 a'_1 a_1)^H + \\ \left(-g_2 g_1 a_2 a_1^H (g'_1 a_1 + g_1 a'_1 a_1) + g_1^2 (g'_2 a_2 + g_2 a'_2 a_2)\right) (g'_2 a_2 + g_2 a'_2 a_2)^H \end{bmatrix} \end{aligned} \tag{26}$$

Thus, the last expression can be divided into two components of its terms. Consider the left (in our case, the top) term:

$$\begin{aligned} &\left(g_2^2 (g'_1 a_1 + g_1 a'_1 a_1) - g_1 g_2 a_1 a_2^H (g'_2 a_2 + g_2 a'_2 a_2)\right) (g'_1 a_1 + g_1 a'_1 a_1)^H = \\ &g_2^2 (g'_1 a_1 + g_1 a'_1 a_1) (g'_1 a_1 + g_1 a'_1 a_1)^H + g_1 g_2 a_1 a_2^H (g'_2 a_2 + g_2 a'_2 a_2) (g'_1 a_1 + g_1 a'_1 a_1)^H = \\ &g_2^2 \left(g'_1 a_1 g'_1 a_1^H + g_1 a'_1 a_1 g'_1 a_1^H + g'_1 a_1 g_1 a'^H_1 a_1^H + g_1 a'_1 a_1 g_1 a'^H_1 a_1^H\right) + \\ &\left(-g_1 g_2 a_1 a_2^H\right) \left(g'_2 a_2 g'_1 a_1^H + g_2 a'_2 a_2 g'_1 a_1^H + g'_2 a_2 g_1 a'^H_1 a_1^H + g_2 a'_2 a_2 g_1 a'^H_1 a_1^H\right) = \\ &g_2^2 \left(g'^2_1 + g_1 g'_1 a'_1 + g'_1 g_1 a'^H_1 + g_1^2 a'_1 a'^H_1\right) + \\ &\left(-g_1 g_2 a_1 a_2^H\right) \left(g'_2 a_2 g'_1 a_1^H + g_2 a'_2 a_2 g'_1 a_1^H + g'_2 a_2 g_1 a'^H_1 a_1^H + g_2 a'_2 a_2 g_1 a'^H_1 a_1^H\right) = \\ &g_2^2 \left(g'^2_1 + g_1^2 a'_1 a'^H_1\right) + \\ &(-1) \left(g_1 g_2 a_1 a_2^H g'_2 a_2 g'_1 a_1^H + g_1 g_2 a_1 a_2^H g_2 a'_2 a_2 g'_1 a_1^H + g_1 g_2 a_1 a_2^H g'_2 a_2 g_1 a'^H_1 a_1^H \right. \\ &\left. + g_1 g_2 a_1 a_2^H g_2 a'_2 a_2 g_1 a'^H_1 a_1^H\right) = \\ &g_2^2 \left(g'^2_1 + g_1^2 a'_1 a'^H_1\right) + (-1) \left(g_1 g_2 g'_2 g'_1 + g_1 g_2^2 g'_1 a'_2 + g_1^2 g_2 g'_2 a'^H_1 + g_1^2 g_2^2 a'_2 a'^H_1\right) \end{aligned} \tag{27}$$

Now consider the right (in our case, the lower) addend:

$$\begin{aligned} &\left(-g_2 g_1 a_2 a_1^H (g'_1 a_1 + g_1 a'_1 a_1) + g_1^2 (g'_2 a_2 + g_2 a'_2 a_2)\right) (g'_2 a_2 + g_2 a'_2 a_2)^H = \\ &-g_2 g_1 a_2 a_1^H (g'_1 a_1 + g_1 a'_1 a_1) (g'_2 a_2 + g_2 a'_2 a_2)^H + g_1^2 (g'_2 a_2 + g_2 a'_2 a_2) (g'_2 a_2 + g_2 a'_2 a_2)^H = \\ &(-1) \left(g_2 g_1 a_2 a_1^H\right) \left(g'_1 a_1 g'_2 a_2^H + g_1 a'_1 a_1 g'_2 a_2^H + g'_1 a_1 g_2 a'^H_2 a_2^H + g_1 a'_1 a_1 g_2 a'^H_2 a_2^H\right) + \\ &g_1^2 \left(g'_2 a_2 g'_2 a_2^H + g_2 a'_2 a_2 g'_2 a_2^H + g'_2 a_2 g_2 a'^H_2 a_2^H + g_2 a'_2 a_2 g_2 a'^H_2 a_2^H\right) = \\ &(-1) (g_2 g_1) \left(g'_1 g'_2 + g_1 a'_1 g'_2 + g'_1 g_2 a'^H_2 + g_1 a'_1 g_2 a'^H_2\right) + g_1^2 \left(g'^2_2 + g_2^2 a'_2 a'^H_2\right) \end{aligned} \tag{28}$$

Now consider the sum of the terms:

$$
\begin{array}{l}
g_2^2\left(g'^2_1+g_1^2a'_1a'^H_1\right)+(-1)\left(g_1g_2g'_2g'_1+g_1g_2^2g'_1a'_2+g_1^2g_2g'_2a'^H_1+g_1^2g_2^2a'_2a'^H_1\right)+\\
(-1)\left(g_2g_1\right)\left(g'_1g'_2+g_1a'_1g'_2+g'_1g_2a'^H_2+g_1a'_1g_2a'^H_2\right)+g_1^2\left(g'^2_2+g_2^2a'_2a'^H_2\right)=\\
\left[g_2^2\left(g'^2_1+g_1^2a'_1a'^H_1\right)+g_1^2\left(g'^2_2+g_2^2a'_2a'^H_2\right)\right]+\\
(-1)\left[\begin{array}{l} g_1g_2g'_2g'_1+g_1g_2^2g'_1a'_2+g_1^2g_2g'_2a'^H_1+g_1^2g_2^2a'_2a'^H_1+g'_1g'_2g_2g_1+g_1g'_2g_2g_1a'_1+g'_1g_2g_2g_1a'^H_2+\\ g_2g_1g_1g_2a'_1a'^H_2\end{array}\right]=\\
\left[\left(g'^2_1g_2^2+g_1^2g_2^2a'_1a'^H_1\right)+\left(g'^2_2g_1^2+g_2^2g_1^2a'_2a'^H_2\right)\right]+\\
(-1)\left[\begin{array}{l} g_1g_2g'_2g'_1+g_1g_2^2g'_1a'_2+g_1^2g_2g'_2a'^H_1+g_1^2g_2^2a'_2a'^H_1+g'_1g'_2g_2g_1+g_1^2g'_2g_2a'_1+g'_1g_2^2g_1a'^H_2+\\ g_2^2g_1^2a'_1a'^H_2\end{array}\right]=\\
\left[g'^2_1g_2^2+g_1^2g_2^2a'_1a'^H_1+g'^2_2g_1^2+g_2^2g_1^2a'_2a'^H_2\right]+\\
(-1)\left[\begin{array}{l} (g_1g_2g'_2g'_1+g'_1g'_2g_2g_1)+\left(g_1g_2^2g'_1a'_2+g'_1g_2^2g_1a'^H_2\right)+\left(g_1^2g_2g'_2a'^H_1+g_1^2g'_2g_2a'_1\right)+\\ \left(g_1^2g_2^2a'_2a'^H_1+g_2^2g_1^2a'_1a'^H_2\right)\end{array}\right]=\\
g'^2_1g_2^2+g_1^2g_2^2a'_1a'^H_1+g'^2_2g_1^2+g_2^2g_1^2a'_2a'^H_2-2g_1g_2g'_2g'_1+2g_1^2g_2^2a'_2a'_1=\\
\left(g_1^2g_2^2a'_1a'^H_1+2g_1^2g_2^2a'_2a'_1+g_2^2g_1^2a'_2a'^H_2\right)+\left(g'^2_2g_1^2-2g_1g_2g'_2g'_1+g'^2_1g_2^2\right)=\\
g_1^2g_2^2\left(a'_1a'^H_1+2a'_2a'_1+a'_2a'^H_2\right)+\left(g'_2g_1-g'_1g_2\right)^2=g_1^2g_2^2\left(a'_1-a'_2\right)^2+\left(g'_2g_1-g'_1g_2\right)^2
\end{array}
\tag{29}
$$

The following properties have been used to obtain the latest expressions:

1. $a_ia_i^H=0$

   $\left(e^{j\psi_i}\right)\left(e^{j\psi_i}\right)^H=\left(e^{j\psi_i}\right)\left(e^{-j\psi_i}\right)=0$

2. $a'_i+a'^H_i=0$

   $\dfrac{\partial j\mathbf{k}r_i^T}{\partial\eta}+\left(\dfrac{\partial j\mathbf{k}r_i^T}{\partial\eta}\right)^H=\dfrac{\partial j\mathbf{k}r_i^T}{\partial\eta}+(-1)\dfrac{\partial j\mathbf{k}r_i^T}{\partial\eta}=0$

3. $a'_ia'^H_i=\left(\dfrac{\partial j\mathbf{k}r_i^T}{\partial\eta}\right)\left(\dfrac{\partial j\mathbf{k}r_i^T}{\partial\eta}\right)^H=\left(\dfrac{\partial j\mathbf{k}r_i^T}{\partial\eta}\right)(-1)\left(\dfrac{\partial j\mathbf{k}r_i^T}{\partial\eta}\right)=\left(\dfrac{\partial\mathbf{k}r_i^T}{\partial\eta}\right)\left(\dfrac{\partial\mathbf{k}r_i^T}{\partial\eta}\right)=\left(\dfrac{\partial\mathbf{k}r_i^T}{\partial\eta}\right)^2$

4. $a'_ia'_j=\left(\dfrac{\partial j\mathbf{k}r_i^T}{\partial\eta}\right)\left(\dfrac{\partial j\mathbf{k}r_i^T}{\partial\eta}\right)=(-1)\left(\dfrac{\partial\mathbf{k}r_i^T}{\partial\eta}\right)\left(\dfrac{\partial\mathbf{k}r_i^T}{\partial\eta}\right)=(-1)\left(\dfrac{\partial\mathbf{k}r_i^T}{\partial\eta}\right)^2$

Thus:

$$\left(\mathbf{D}^H_{\theta,\varphi}\mathbf{P}^{\perp}_A\mathbf{D}_{\theta,\varphi}\right)=\frac{1}{g_1^2+g_2^2}\left[g_1^2g_2^2\left(a'_1-a'_2\right)^2+\left(g'_2g_1-g'_1g_2\right)^2\right] \tag{30}$$

And then the exact equation of the Cramer-Rao lower bound for a particular antenna array composed of two directional antennas looks like the following:

$$
\begin{array}{l}
\left[\begin{array}{ccc} \mathrm{var}(\theta_1,\varphi_1) & & 0\\ & \ddots & \\ 0 & & var(\theta_M,\varphi_M)\end{array}\right]\\
=\ \dfrac{\sigma^2}{2N}\Re\left[\left(\mathbf{D}^H_{\theta,\varphi}\mathbf{P}^{\perp}_A\mathbf{D}_{\theta,\varphi}\right)\circ\Xi\right]^{-1}=\dfrac{\sigma^2}{2N}\Re\left[\dfrac{1}{g_1^2+g_2^2}\left[g_1^2g_2^2\left(a'_1-a'_2\right)^2+\left(g'_2g_1-g'_1g_2\right)^2\right]\circ\Xi\right]^{-1}
\end{array}
\tag{31}
$$

Because of the special case, we get that $\Xi \approx P_S \approx g_1^2 + g_2^2$, and it follows:

$$\begin{aligned}
&\begin{bmatrix} \mathrm{var}(\theta_1,\varphi_1) & & 0 \\ & \ddots & \\ 0 & & \mathrm{var}(\theta_M,\varphi_M) \end{bmatrix} = \frac{\sigma^2}{2N}\Re\left[\left(\mathbf{D}_{\theta,\varphi}^H \mathbf{P}_A^{\perp} \mathbf{D}_{\theta,\varphi}\right) \circ \Xi\right]^{-1} \\
&\approx \frac{\sigma^2}{2N}\Re\left[\frac{1}{g_1^2+g_2^2}\left[g_1^2 g_2^2 \left(a'_1 - a'_2\right)^2 + \left(g'_2 g_1 - g'_1 g_2\right)^2\right] \circ \left(g_1^2+g_2^2\right)\right]^{-1} \\
&\approx \frac{\sigma^2}{2N}\Re\left\{\frac{1}{g_1^2 g_2^2 \left(a'_1 - a'_2\right)^2 + \left(g'_2 g_1 - g'_1 g_2\right)^2}\right\} \qquad (32)
\end{aligned}$$

From the last expression (32) it can be seen that the DOA-estimation accuracy using antenna arrays composed of directional elements is higher if the square of the phase differences is bigger together with the square of the difference between their radiation patterns and additionally the square of their radiation patterns. The phase difference is caused by the positions in space of the individual elements. Or in other words, CRLB is mainly determined by two terms: firstly, the square of phase differences determined by the positions of the antennas, and secondly, the square of radiation patterns of each individual element.

Knowing formula (32), it is possible to obtain such arrangement of antenna elements in space and their radiation patterns that the term AR would be maximal, and thus CRLB will be minimal in azimuth and/or elevation. Now it is time to optimize antenna elements locations in XY plane according to Eq. (15) and angle of rotation of the radiation pattern in azimuth according to Eq. (3) in order to minimize Eq. (32) azimuth DOA estimation errors. In this case, it is assumed for the initial simplification of the task that the signal has a coordinate in the azimuth plane of about 150° and the elevation of 90°. The initial locations of the antenna elements are 0° and 180° in the azimuth plane as shown in Fig. 3(c). Consider also two restrictions of the minimization of Eq. (32): firstly, the antennas will stay in their original positions, but the rotation angle of the radiation patterns will be optimized; the second boundary condition is the angles of rotation of the patterns coincide with the angles of shifts of the antennas as in the common cylindrical arrays depicted in Fig. 1(c). The results of estimating CRLB of Eq. (12) after optimization Eq. (32) in the azimuth are shown in Fig. 3.

After the optimization, the directions of the emitters are 121° and 205°. In this case, the antenna elements themselves stay in the same places, i.e., 0° and 180° (Fig. 3(a)). The emitters rotate only by calculated values. Such an approach can be implemented, but in the authors' opinion, it is poorly realizable. It is more realistic to have a multi-element cylindrical antenna array but with switched elements to scan a specific area of space. For example, we also have two patch antennas and would like to scan the same area, i.e., $\theta = 150°$. After optimization, the elements will be located at a distance R from the center of the array, but their angles of rotations are calculated and are 118° and 212°, respectively (Fig. 3(b)).

From the curves shown in Fig. 3, it is seen that the optimization of the locations of elements makes the DOA errors decrease by several dozen times around $\theta = 150°$ in the azimuth in comparison with the standard cylindrical array (Fig. 3(c)). In addition, the obtained antenna array configurations shown in Figs. 3(a) and 3(b) give approximately the same results. At the same time, due to the obtained optimization results of Equation (32), the RMSE peaks are shifted by 180°. Next, we analyze each component of formula (32), which leads to the results represented in Fig. 3.

After viewing Fig. 4, we can produce or generalize the strategy of optimizing the construction of antenna arrays to reduce the error of DOA estimates. As we can see that the peaks of the left and right terms are offset from each other, it is impossible to achieve a symmetrical arrangement of the two antennas and their radiation patterns in order to reach the maximum accuracy. It is more important to achieve some balance between phase shifts and antenna rotations around the z-axis, which we can see from Fig. 4(b). Furthermore, it is obviously seen why the standard two-element array provides the maximal accuracy at $\theta = 90°$, $\theta = 270°$: their placements are against each other, and overall multiplication tends to zero at $\theta = 0°$ and $\theta = 180°$, unlike other cases.

Consider now the situation, at which it is supposed that the source has a coordinate in the azimuth of 90°. In this case, we will also optimize the placement of antenna elements in space, and the results of the RMSE estimates are shown in Fig. 5.

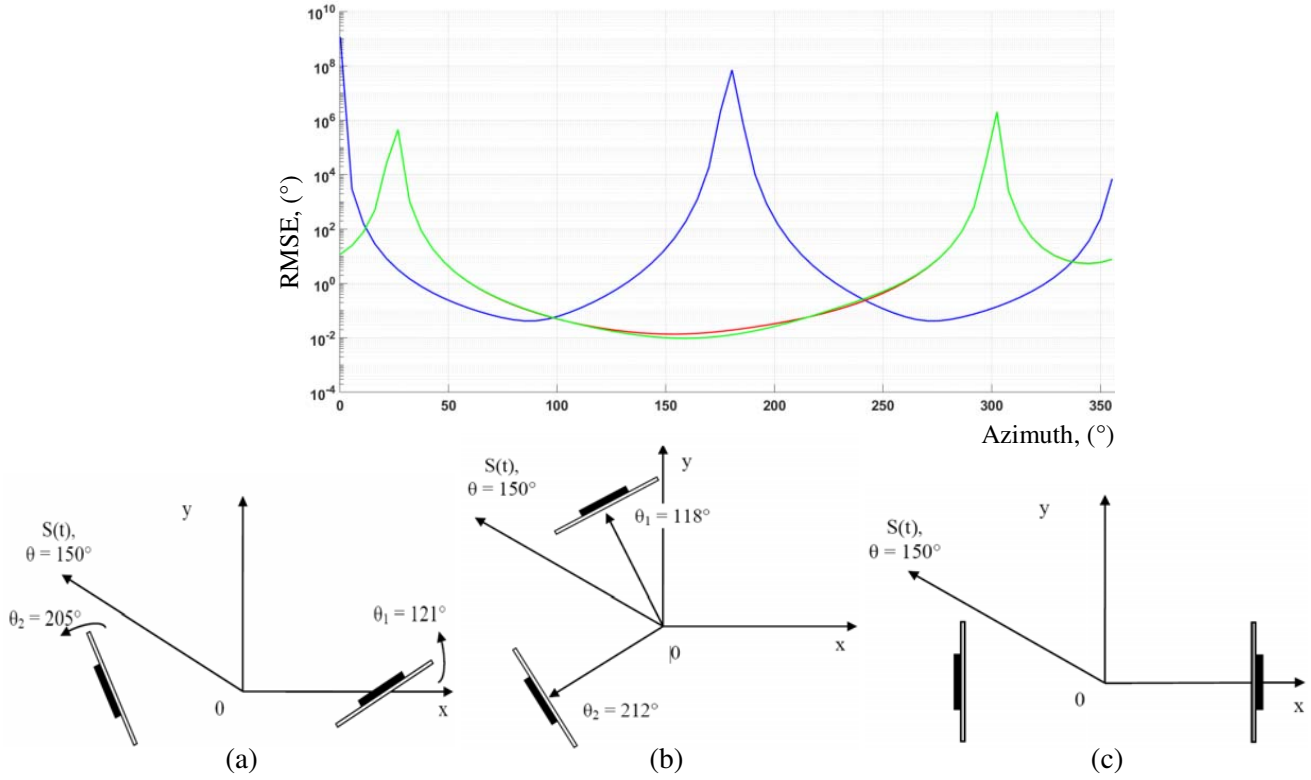

Figure 3. CRLB of two-element antenna array optimized for the source of $\theta = 150°$: (a) the geometry with 121° and 205° rotations relates to the red curve; (b) the geometry with 118° and 212° shifts relates to the green curve; (c) the standard antenna array relates to the blue curve.

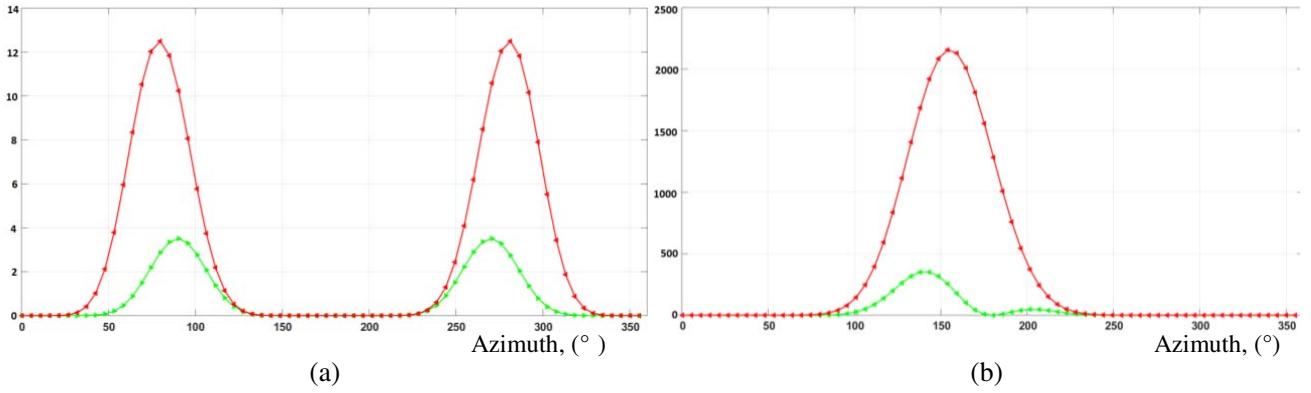

Figure 4. Evaluation of the left (red) and right (green) components of the denominator CRLB (32) of a) Figs. 3(c) and (b) Fig. 3(b) configurations.

It is clearly seen from the RMSE curves in Fig. 5 that minimizing expression (32) also produces the reduction in the DOA errors of the estimates, even for minimal errors of the standard cylindrical two-element antenna array. In addition, Fig. 5(b) shows that the optimization does not give a symmetrical position (as it could be supposed) of elements around $\theta = 90°$ which can help in the design of multi-element cylindrical arrays with switched antennas.

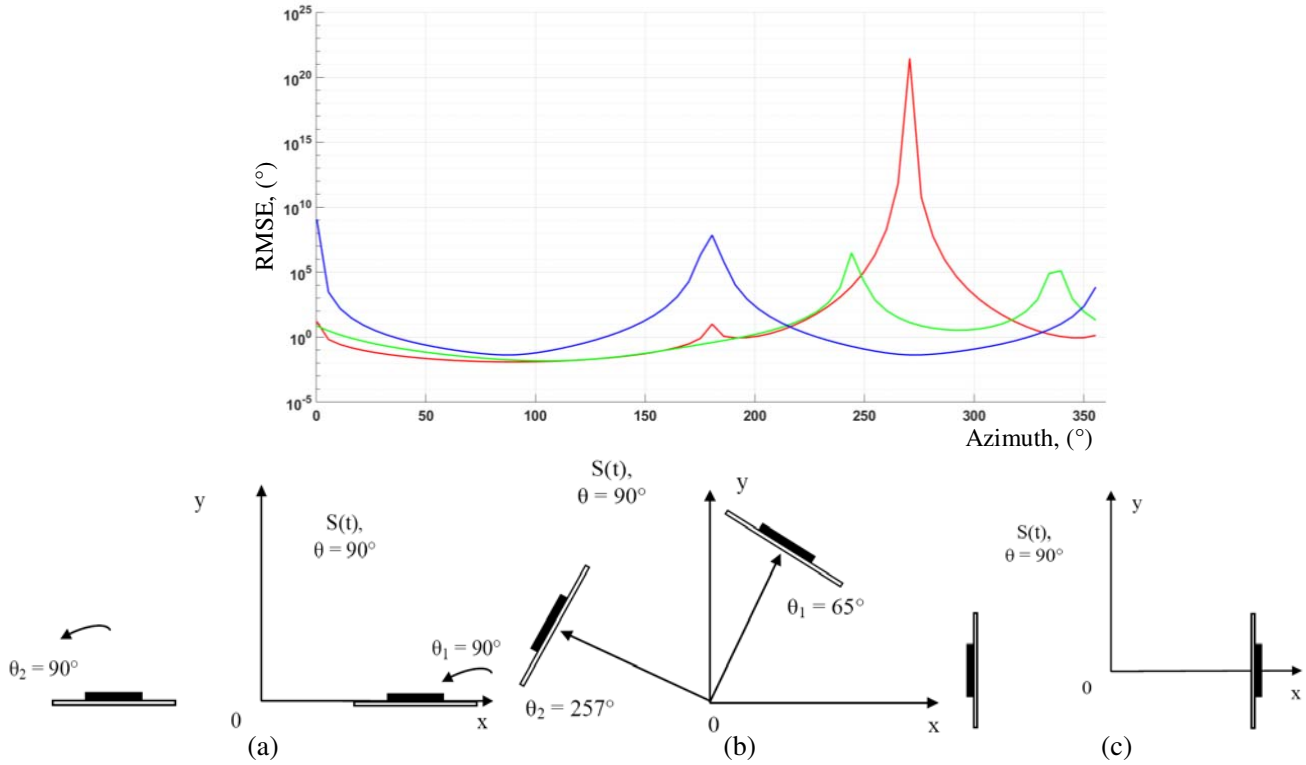

Figure 5. CRLB of two-element antenna array optimized for the source of $\theta = 90°$: (a) the geometry with 90° and 90° antenna rotations relates to the red curve; (b) the geometry with 65° and 157° shifts relates to the green curve, (c) the standard geometry relates to the blue curve.

4.2. The Exact Equation of the CRLB. One Signal and Three Antennas

Now consider a case that a particular antenna array consists of three directional antenna elements and with arbitrary locations, as well as a single source.

$$\begin{bmatrix} \mathrm{var}(\theta_1,\varphi_1) & & 0 \\ & \ddots & \\ 0 & & \mathrm{var}(\theta_M,\varphi_M) \end{bmatrix} = \frac{\sigma^2}{2N}\Re\left[\left(\mathbf{D}^H_{\theta,\varphi}\mathbf{P}^{\perp}_A\mathbf{D}_{\theta,\varphi}\right)\circ\Xi\right]^{-1} \approx$$

$$\frac{\sigma^2}{2N}\Re\left[\begin{array}{l}\dfrac{1}{g_1^2+g_2^2+g_3^2}\left[g_1^2g_2^2\left(a'_1-a'_2\right)^2+g_3^2g_1^2\left(a'_1-a'_3\right)^2+g_3^2g_3^2\left(a'_2-a'_3\right)^2\right.\\ \left.+\left(g'_2g_1-g'_1g_2\right)^2+\left(g'_3g_1-g'_1g_3\right)^2+\left(g'_2g_3-g'_3g_2\right)^2\right]\circ\left(g_1^2+g_2^2+g_3^2\right)\end{array}\right]^{-1} \approx \tag{33}$$

$$\frac{\sigma^2}{2N}\Re\left\{\frac{1}{\left(\begin{array}{l}g_1^2g_2^2\left(a'_1-a'_2\right)^2+g_3^2g_1^2\left(a'_1-a'_3\right)^2+g_2^2g_3^2\left(a'_2-a'_3\right)^2\\+\left(g'_2g_1-g'_1g_2\right)^2+\left(g'_3g_1^-g'_1g_3\right)^2+\left(g'_2g_3-g'_3g_2\right)^2\end{array}\right)}\right\}$$

Let us optimize the arrangement of elements to minimize Eq. (33), and it is assumed that a single signal has the azimuth coordinate of 150° (the results are shown in Fig. 6) and in the second scenario is $\theta = 90°$ (the results are shown in Fig. 7).

It can be seen from Figs. 6 and 7 that the optimal location of the antenna elements and their radiation patterns cannot always be predicted. In other words, it is not always necessary to direct the antenna elements strictly in a particular direction to estimate accurately direction-of-arrivals within the

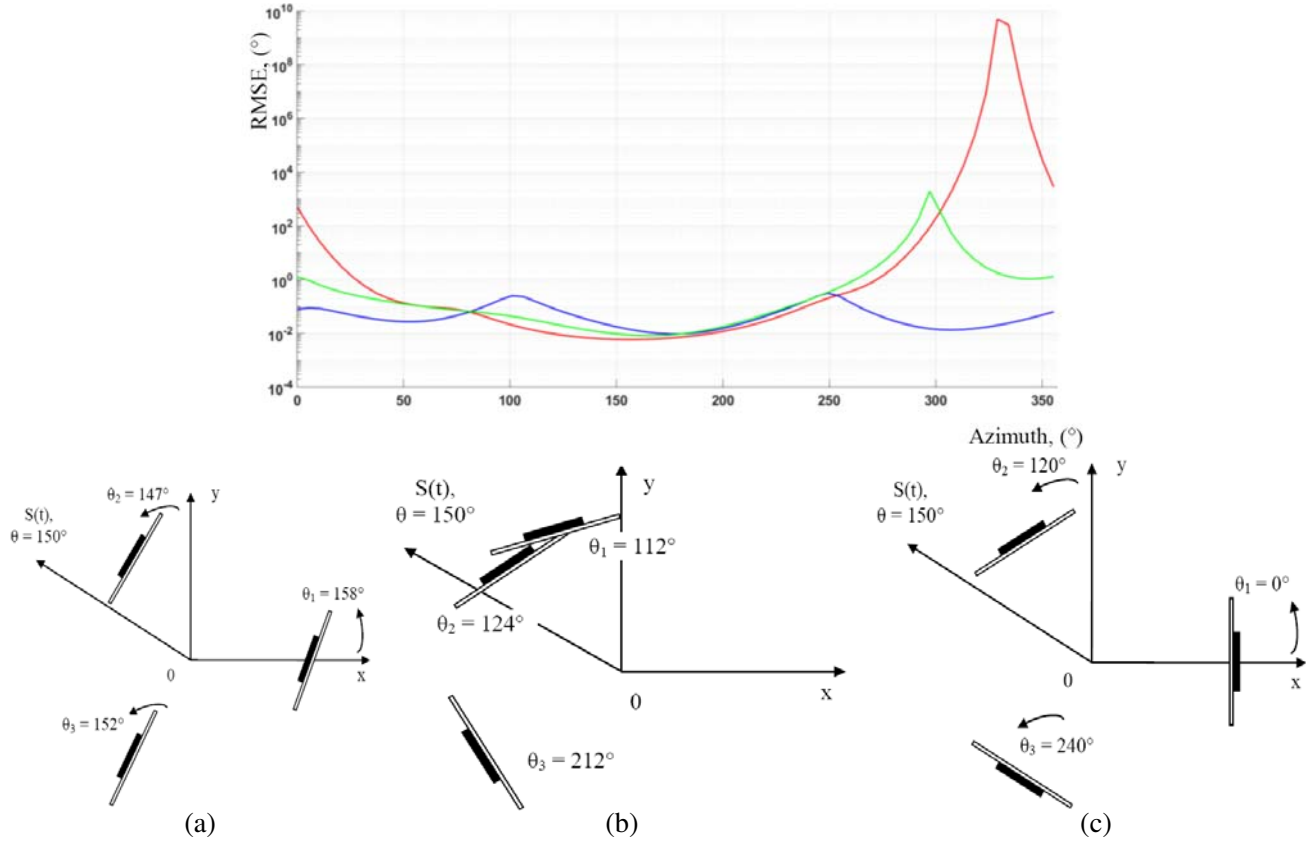

Figure 6. CRLB of three-element antenna array optimized for the source of $\theta = 150°$: (a) the geometry with 158°, 147° and 152° antennas rotations relates to the red curve; (b) the geometry with 112°, 124°, 212° shifts relates to the green curve; (c) the standard array relates to the blue curve.

sector, which is most clearly seen from the configurations in Figs. 6(b), 7(a), (b). In addition, the square of the phase differences multiplied by the square of the spatial patterns plays the most important role, and this term gives significant values in the denominator of formula (32), as it can be clearly seen from the configurations of the antenna arrays depicted in Figs. 6(b) and 7(b).

4.3. The General Expression of the CRLB for a Particular Antenna Array with Directional Elements

Thus, it is rather easy to derive the general expression of the CRLB for DOA-estimation on the azimuth and elevation using particular antenna arrays with an arbitrary number of directional elements, oriented in space also randomly:

$$\begin{bmatrix} \mathrm{var}(\theta_1, \varphi_1) & & 0 \\ & \ddots & \\ 0 & & \mathrm{var}(\theta_M, \varphi_M) \end{bmatrix} = \frac{\sigma^2}{2N} \Re \left[\left(\mathbf{D}^H_{\theta,\varphi} \mathbf{P}^{\perp}_A \mathbf{D}_{\theta,\varphi} \right) \circ \Xi \right]^{-1}$$

$$\approx \frac{\sigma^2}{2N} \Re \left\{ \frac{1}{\sum\limits_{ij} g_i^2 g_j^2 \left(a'_i - a'_j \right)^2 + \sum\limits_{ij} \left(g'_i g_j - g'_j g_i \right)^2} \right\} \tag{34}$$

where $i = 1 \div N$, $j = 1 \div N$, $i \neq j$.

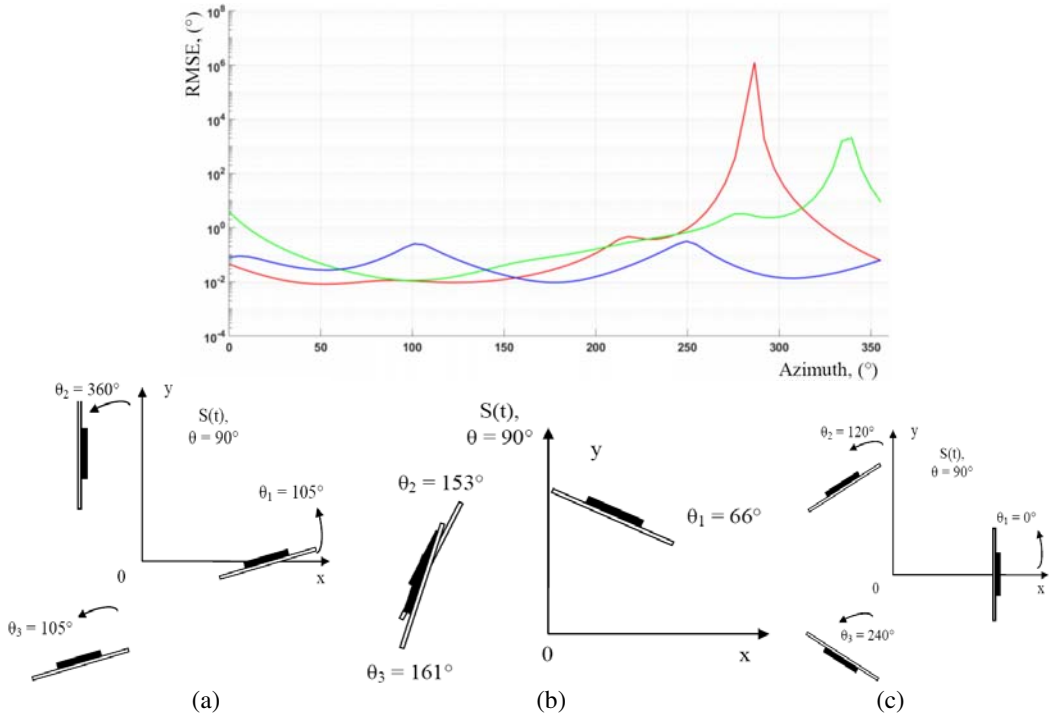

Figure 7. CRLB of three-element antenna array optimized for the source of $\theta = 90°$: (a) the geometry with 105°, 360°, 105° antennas rotations relates to the red curve; (b) the geometry with 66°, 153°, 161° shifts relates to the green curve, (c) the standard array relates to the blue curve.

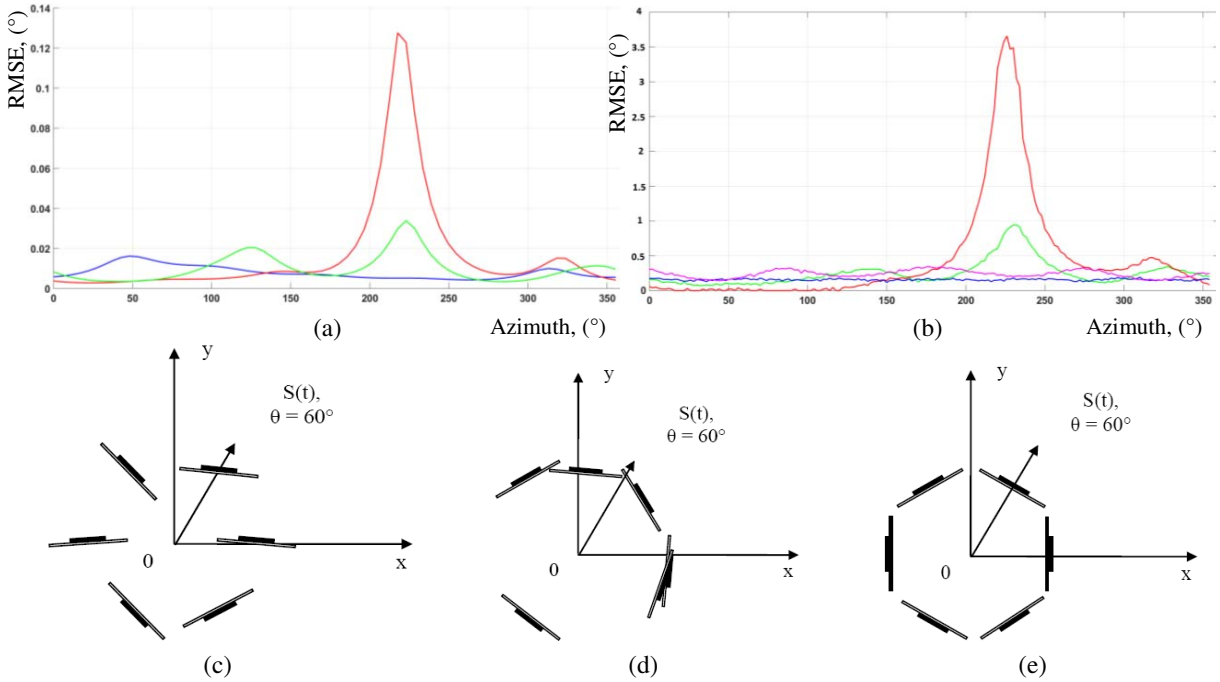

Figure 8. CRLB (a) and MUSIC (b) estimations of six-element antenna array optimized for the source of $\theta = 60°$: (c) the geometry with 86°, 85°, 44°, 94°, 225°, 355° antennas rotations relates to the red curve; (d) the geometry with 41°, 85°, 120°, 232°, 341°, 355° shifts relates to the green curve; (e) the standart array relates to the blue curve. The magenta curve relates to the half-sphere array from Fig. 1(b).

Now consider the situation with a single signal source placed in the area of $\theta = 60^\circ$ and an antenna array with six elements, as in the first example above. In addition, we take the semi-spherical array depicted in Fig. 1(b) for estimating the difference in the accuracy of the direction finding in comparison with the initial cylindrical one. In addition to the theoretical studies, we present some numerical simulation results to illustrate the effectiveness of the optimized antenna array configurations for the direction-of-arrival estimation with super-resolution using the MUSIC method [4].

We can see from Fig. 8 that the RMSE of the MUSIC method coincides in shape with the RMSE of the Cramer-Rao lower bound. It is also obvious that the obtained configurations of the antenna arrays allow reducing the errors of DOA estimation lower than those values of both the standard cylindrical array and the half-sphere one. It can also be said that the optimal scanning for radio direction finding in a certain sector is achieved if small groups of antenna elements are located around two to three points to ensure high mutual values of the phase differences as well as the product of the squares of the directivity patterns as it is particularly noticeable from Fig. 8(d). In this case, the denominator of Equation (34) will reach a maximal value and therefore will lead to greater accuracy, which can also be seen from the results of the numerical simulation of the MUSIC method (Fig. 8(b)).

5. CONCLUSIONS

Conformal or volume antenna arrays consist of antenna elements, placed on a curved ground. These kinds of arrays of sensors are of research interest for direction finding and wireless communication because they are capable of processing signals in a three-dimensional plane (the azimuth and elevation) and can be mounted on objects of complex shape such as cars and airplanes.

In the paper, the antenna arrays of different configurations have been researched depending on the directivity factor of each antenna element. The cylindrical, cubic, sphere, and cone antenna array geometries have been chosen under consideration. They have the same number of antennas and occupy the comparable area. It is established that the array in the form of a half-sphere has minimal errors in DOA estimation tasks on azimuth and elevation.

The adaptation of the Cramer-Rao boundary expression for the 3D direction-finding tasks of conformal antenna arrays with directive emitters is carried out. The influence of the azimuth and elevation coordinates of radio emission sources on the accuracy of radio direction finding is estimated. It is established that significantly increasing the directivity of the antenna elements leads to big errors in DOA estimates. Using the exact equation of the Cramer-Rao lower bound could help to produce such antenna arrays configurations which significantly allow improving the accuracy in a given sector. The proposed technique will allow using antenna arrays with switched scanning sectors with greater efficiency.

ACKNOWLEDGMENT

The work is supported by RSF. The project number is 18-71-00080.

REFERENCES

1. Chetan, R. D. and A. N. Jadhav, "Simulation study on DOA estimation using MUSIC algorithm," *Intl. J. Tech. Eng. Sys.*, Vol. 2, No. 1, Mar. 2011.
2. Ikeda, K., J. Nagai, T. Fujita, H. Yamada, A. Hirata, and T. Ohira, "DOA estimation by using MUSIC algorithm with a 9-elements rectangular ESPAR antenna," *Proc. of Intl. Symp. on Antennas and Propagat.*, 45–48, Aug. 2004.
3. Sun, C. and N. C. Karmakar, "Direction of arrival estimation based on a single port smart antenna using MUSIC algorithm with periodic signals," *Intl. J. Signal Process.*, Vol. 1, No. 3, 153–162, 2010.
4. Schmidt, R. O., "Multiple emitter location and signal parameter estimation," *IEEE Trans. Antennas Propagat.*, Vol. 34, 276–280, 1986.

5. Belhoud, F. A., R. M. Shubair, and M. E. Al-Mualla, "Modelling and performance analysis of DOA estimation in adaptive signal processing arrays," *Proc. IEEE Intl. Conf. on Electron., Circuits and Sys.*, 340–343, Dec. 2003.
6. Cadzow, J. A., "A high resolution direction-of-arrival algorithm for narrow-band coherent and incoherent sources," *IEEE Trans. Acoust., Speech, Signal Process.*, Vol. 36, No. 7, 965–979, Jul. 1998.
7. Abouda, A., H. M. El-Sallabi, and S. G. Haggman, "Impact of antenna array geometry on MIMO channel eigenvalues," *Proc. IEEE Intl. Symp. on Personal, Indoor and Mobile Radio Comm.*, Vol. 1, 568–572, Sep. 2005.
8. Nechaev, Y. and I. Peshkov, "Building circular, octagonal, hexagonal and rectangular antenna arrays for direction-of-arrival via superresolutional method MUSIC," *Radioengineering*, No. 6, 137–142, 2016.
9. Wu, B., "Realization and simulation of DOA estimation using MUSIC algorithm with uniform circular arrays," *The 4th Asia-Pacific Conf. on Environmental Electromagnetics*, 908–912, 2006.
10. Nechaev, Yu. B. and I. V. Peshkov, "Evaluating Cramer-Rao Bound for 2D direction-finding via planar antenna arrays," *Visn. NTUU KPI, Ser. Radioteh. Radioaparatobuduv.*, No. 67, 12–17, 2016.
11. Jackson, B. R., S. Rajan, B. J. Liao, and S. Wang, "Direction of arrival estimation using directive antennas in uniform circular arrays," *IEEE Transactions on Antennas and Propagation*, Vol. 63, No. 2, 736–747, 2015.
12. Mohammadi, S., A. Ghani, S. H. Sedighy, "Direction of arrival estimation in conformal microstrip patch array antenna," *IEEE Transactions on Antennas and Propagation*, Vol. 66, No. 1, 511–515, 2018.
13. Gazzah, H., J.-P. Delmas, and S. M. Jesus, "Direction-finding arrays of directional sensors for randomly located sources," *IEEE Transactions on Aerospace and Electronic Systems*, Vol. 52, 1995–2003, 2016.
14. Gazzah, H. and S. Marcos, "Directive antenna arrays for 3D source localization," *4th IEEE Workshop on Signal Processing Advances in Wireless Communications, 2003. SPAWC 2003*, 619–623, 2003.
15. Chan, A. Y. J. and J. Litva, "MUSIC and maximum likelihood techniques on two-dimensional DOA estimation with uniform circular array," *IEE Proceedings — Radar, Sonar and Navigation*, Vol. 142, No. 3, 105–114, 2018.
16. Nechaev, Yu. B., E. Algazinov, and I. Peshkov, "Estimation of the cramer-rao bound for radio direction-finding on the azimuth and elevation of the cylindical antenna arrays," *41st International Conference on Telecommunications and Signal Processing (TSP)*, DOI: 10.1109/TSP.2018.8441419, 2018.
17. Moriya, H., et al., "Novel 3-D array configuration based on CRLB formulation for high-resolution DOA estimation," *Proceedings of ISAP 2012*, 1140–1143, Nagoya, Japan, 2012.